Eur. Phys. J. Special Topics **224**, 3311–3323 (2015)

DOI: 10.1140/epjst/e2015-50082-8

THE EUROPEAN PHYSICAL JOURNAL SPECIAL TOPICS

Regular Article

The shape and dynamics of local attraction

D. Strömbom[1,3,a], M. Siljestam[2], J. Park[3], and D.J.T. Sumpter[3]

[1] Department of Biology, Lafayette College, Easton, PA, USA
[2] Department of Ecology and Genetics, Uppsala University, Uppsala, Sweden
[3] Department of Mathematics, Uppsala University, Uppsala, Sweden

Received 14 April 2015 / Received in final form 2 November 2015
Published online 15 December 2015

Abstract. Moving animal groups, such as flocks of birds or schools of fish, exhibit a varity of self-organized complex dynamical behaviors and shapes. This kind of flocking behavior has been studied using self-propelled particle models, in which the "particles" interact with their nearest neighbors through repulsion, attraction and alignment responses. In particular, it has been shown that models based on attraction alone can generate a range of dynamic groups in 2D, with periodic boundary conditions, and in the absence of repulsion. Here we investigate the effects of changing these conditions on the type of groups observed in the model. We show that replacing the periodic boundary conditions with a weak global attaction term in 2D, and extending the model to 3D does not significantly change the type of groups observed. We also provide a description of how attraction strength and blind angle determine the groups generated in the 3D version of the model. Finally, we show that adding repulsion do change the type of groups oberved, making them appear and behave more like real moving animal groups. Our results suggest that many biological instances of collective motion may be explained without assuming that animals explicitly align with each other. Instead, complex collective motion is explained by the interplay of attraction and repulsion forces.

1 Introduction

Natural moving animal groups come in many different forms and exhibit different dynamical properties. Typical shapes range from mills, tori, balls, more or less elongated sheets and tubes/strings via hybrids of these to seemingly randomly scattered individuals [1–3]. The overall shape of a flock may change either spontaneously or as a result of changing environmental conditions, such as predator attacks [4]. In some cases, this shape-shifting may also include splitting and merging of the flock. Inside some flocks the relative position of individuals is fixed whereas in others repositioning of individuals, or subgroups, within the group occur [1,3,5–8]. The preferred separation between flock members can vary significantly. In some, individuals are kept apart

[a] e-mail: stroembp@lafayette.edu

by physical size only [9,10] and in others they are more sparsely distributed, often with a preferred inter-individual distance [8,11–14].

Flocking patterns vary greatly between species. For example, surf scoters paddle on the surface of the water in slow moving regular groups [15,16]. These groups are characterized by distinct inter-individual spacing, "follow the leader" type interactions and a crystal-like formation. The group may change form depending on situation, from more round to a string like chain. Unlike the stable patterns seen in surf scoters, flying starlings form flocks capable of moving synchronously and quickly responding to spontaneous or predator induced perturbations [4,8,17]. In addition, some moving animal groups are known to regularly switch between two, or more, shapes over time. For example, golden shiner schools exhibit frequent switching between being in a milling state and a translationally moving state [18].

A number of so called self-propelled particle (SPP) models have been proposed to explain how local interactions can produce large scale flocking patterns [16,19–32]. The main differences between these models lie in how the neighbors of a focal particle is determined and the social forces involved in the local interaction rule. The interaction rule typically depends on a few directional components, from aligning with neighbors alone in [21] to alignment, attraction and repulsion in e.g. [19,20,24]. In many models the distance between individuals defines zones within which individuals are repelled, attracted, or try to align with each other. Most of these models assume that individuals change their orientation in response to the orientation of their neighbors. For a review of collective motion and SPP-models see [33].

The questions we address here relate to whether attraction forces could be the primary driving force in many moving animal groups observed in Nature. One of the remaining modeling challenges include producing groups that exhibit internal repositioning of particles coupled with translational motion. Previously we proposed a self-propelled particle model in which the only social force between individuals is attraction [30]. In 2D this model generates the three standard groups: swarms, mills, and translationally moving (dynamic) groups. Restricting the field of vision, i.e. introducing a blind zone, and increasing the degree of noise resulted in directed mills, strings of various lengths, and three dynamically moving, "rotating chain" groups. While these groups exhibit rich dynamics they are generated in one particular implementation of the model. Using periodic boundary conditions, particle motion restricted to 2D, and no repulsion between particles. Investigating the first two of these implementation choices will inform us about the capacity of the local attraction model [30] as a theoretical tool, and including repulsion will inform us about the potential of using the local attraction model supplemented with repulsion to model real moving animal groups.

A key question is how adding repulsion to the local attraction model will affect the group types generated. More specifically, will groups of the following types form. The standard group types, i.e. swarm, mill, and translationally moving (dynamic) groups. Groups exhibiting translational motion coupled with internal rearrangement of particles, as exemplified by the figure of eight in the attraction only model. Groups that exhibit frequent switching between standard group types, as observed in golden shiner schools [18]. A wide variety of attraction-repuslion models exist in the literature [26,28,29,34–38]. Although the implementation of attraction and repulsion differ, each is known to produce translationally moving groups, and most report observing milling groups. However, few report translationally moving groups exhibiting frequent repositioning of particles, or subgroups, within the main group. Possible exceptions include [29,35] and these models will be contrasted with our current work in the discussion. In addition, to our knowledge no model report observing the type of switching behavior described in [18].

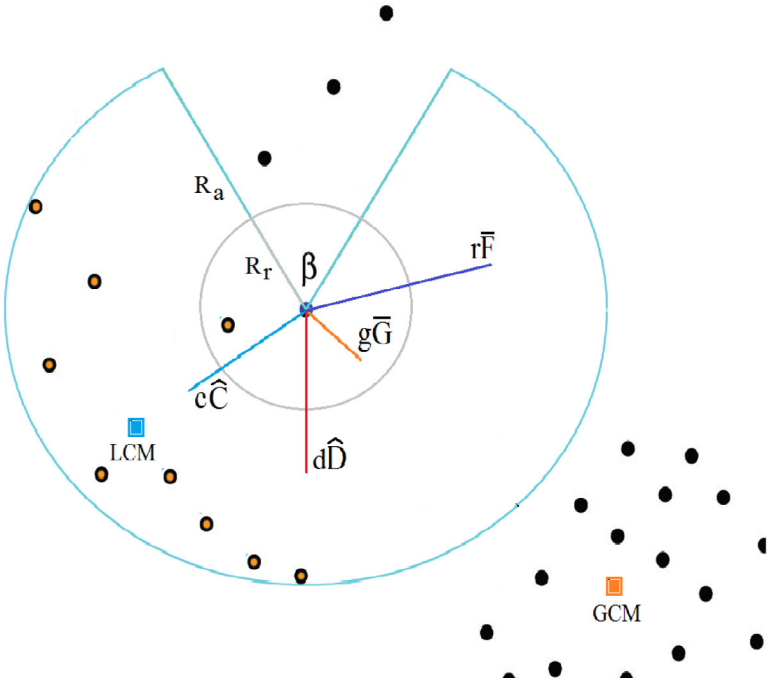

Fig. 1. How a particle calculates its new heading. The tendency to proceed in previous direction vector dD and the attraction to the global center of mass gG are independent of the local neighborhood. The local attraction vector cC has length c and is pointing towards the center of mass (LCM) of all particles within a distance R_a and not in the blind zone specified by β of the focal particle. The local repulsion vector rF is an r-multiple of the distance dependent repulsion vector F defined by equation 5. There is no blind zone for the repulsion. The new heading of the particle is then given by the sum of these four vectors plus some small angular noise (Eq. (6)) and the particle will move a distance δ in this direction.

2 Results

A full description of our model can be found in the model and methods section. In short, we model N identical particles that move with average speed δ in 2 or 3-dimensional space. The heading of particle i in the next time step $\hat{D}_{i,t+1}$ depends on its direction in the previous time step $\hat{D}_{i,t}$, attraction toward the local center of mass of its neighbors $\hat{C}_{i,t}$, and a local repulsion term $F_{i,t}$ (Fig. 1). The center of mass upon which attraction acts is calculated only over those particles within a distance R_a of the focal particle, and excludes those in a blind zone behind the particle specified by the blind angle β. Repulsion is calculated from the positions of all neighbours within a distance $R_r \leq R_a$ and is distance dependent, with nearby neighbors being more repulsive than those further away. To each of the vectors, $\hat{D}_{i,t}$, $\hat{C}_{i,t}$ and $F_{i,t}$ we attach a corresponding weight d, c and r which specifies the relative strength of each term.

Particles only form groups when the density is sufficiently high for local interactions to occur [21]. In [30] we used periodic boundary conditions to keep particles together for sufficiently long periods of time for groups to form. One might argue that this is a somewhat unnatural assumption for real flocks, and it cannot be ruled out that it influences group formation in the model. As a first step here we replace the periodic boundary conditions with a weak linear global attraction term gG to ensure that the density is sufficiently high for local interactions to occur. To model

Table 1. The parameters of the model. Notation, description and typical values used in simulations. Superscripts indicate in which part of the work the parameter value(s) is used. 1: 3D no repulsion, 2: 2D with repulsion, 3: 3D with repulsion.

Parameter	Description	Typical values
L	Side length of initial particle release square/cube	$30^1, 100^{2,3}$
N	Total number of particles	$50^1, 80^2, 100^3$
R_a	Interaction radius for attraction	$10^1, 6^{2,3}$
R_r	Interaction radius for repulsion	$3^{2,3}, 5^{2,3}$
β	Blind angle behind the particle	$0 - 2\pi^{1,2,3}$
c	Relative strength of local attraction	$0 - 1^{1,2,3}$
d	Relative strength of proceeding in previous direction	$1 - c^{1,2,3}$
r	Relative strength of repulsion from other agents	$0.25 - 2^{2,3}$
g	Relative strength of attraction to the global center of mass	$1/20^1, 1/100^{2,3}$
e	Relative strength of angular noise	$1/60^{1,2,3}$
δ	Particle speed	$1^1, 0.5^{2,3}$
κ	Bound on size of variation in particle speed	$1/5^{1,2,3}$

fluctuations in particle movements a small angular noise term $e\hat{\epsilon}_{i,t}$ is included. We study two versions of this model, the attraction only version in which the heading update formula is

$$D_{i,t+1} = d\hat{D}_{i,t} + c\hat{C}_{i,t} + gG + e\hat{\epsilon}_{i,t},$$

and the attraction-repulsion version where the heading update formula is

$$D_{i,t+1} = d\hat{D}_{i,t} + c\hat{C}_{i,t} + rF_{i,t} + gG + e\hat{\epsilon}_{i,t}.$$

A list of all parameters, a brief description of each, and typical values used here may be found in Table 1.

2.1 Attraction only ($r = 0$)

We find that replacing the periodic boundary conditions used in [30] with a free space model including a weak global attraction term does not change the types of groups we see in 2D. The weak global attraction version also produce strings of different lengths, directed mills and rotating chains if the blind angle β is large enough (> 0.1 radians). If the blind angle is small we observe swarms, undirected mills and strings.

In the 3D version we observe analogs of the groups seen in 2D. Movie 1 shows the types of groups generated in simulations. Strings of various lengths are found when the blind angle β and local attraction c are both intermediate to large (Fig. 2a). Mills occur for intermediate to small blind angle β over a wide range of c (Fig. 2b). There are two qualitatively different figures of eight produced by the model. One larger that forms when c is relatively low and β intermediate and one smaller that forms when c is intermediate to high and β intermediate to low (Fig. 2c). Rotating chains occur for c values slightly lower than those which produce a figure of eight, that is c relatively low and β intermediate (Fig. 2d). Swarms form when the blind angle β is small and local attraction c is very strong (not shown in Fig. 2).

To quantify the simulation results we use two measures, see the model and methods section for a full description. First we measure how aligned (or polarized) the group is using the well known alignment measure

$$\alpha = \frac{1}{N}\left|\sum_{i=1}^{N} \hat{D}_i\right|$$

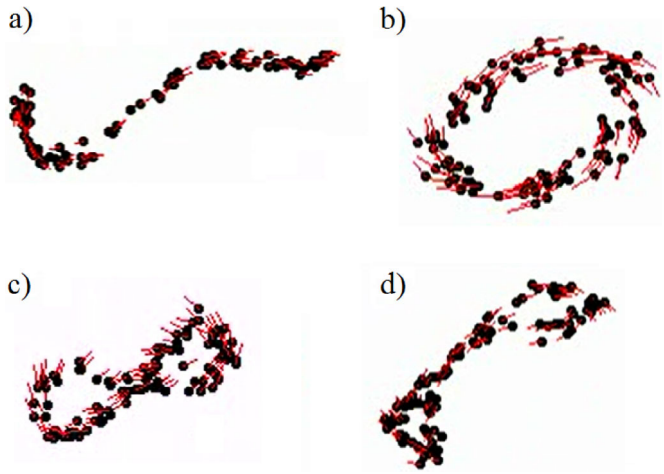

Fig. 2. Snapshots of different phases in the 3D attraction only model. a) String. b) Mill. c) Figure of eight. d) Rotating chain. See Table 1 for the typical parameters used in 3D attraction only simulations, and Movie 1.

where $\hat{D}_i$ is the normalized heading of particle i [21,24]. Then we measure how well the resulting shape can be fitted to a degree two polynomial surface via the non-flatness measure

$$\eta = \log \frac{\sqrt{\sum_{i=1}^{N} \delta_i^2}}{\sqrt{\sum_{i=1}^{N} \rho_i^2}}.$$

where δ_i is the distance from particle i to the nearest point on the fitted surface and ρ_i is the distance from particle i to the group's center of mass. Combining the result of the alignment and non-flatness measures in Fig. 3 we can effectively distinguish regions in the (c, β)-plane and construct a diagram showing where each group type form (Fig. 4a). More precisely, for each (c, β)-pair we have information about the mobility (α) and the three-dimensionality (η) of the resulting group. For example, in the lower right corner of Fig. 3a we see a region with alignment value about $\alpha = 0.2$ and the corresponding region in Fig. 3b has a large non-flatness value $\eta > 1.5$. So in this region we have barely moving groups with three-dimensional structure, which we identify as swarms. Another example is the homogeneous region around $\beta = 4$ radians and $c \in [0.45, 1]$. Figure 3a shows that the alignment is very high (≈ 1) and Fig. 3b reveal that in this same region the non-flatness is very low. We identify these very aligned, very flat groups as strings. Systematically going through Fig. 3a and 3b in this manner and drawing boundaries between the regions identified we obtain the diagram in Fig. 4a. In addition, we produced a scatter plot in the (α, η) plane to allow identification of each group type by its properties and obtain a better understanding of near boundary behavior (Fig. 4b).

2.2 Attraction and repulsion ($r > 0$)

When repulsion is introduced into the model stable rotating chains are no longer observed. Instead, we find more spatially extended groups without self-intersections in which inter-individual distance is maintained. Some of these groups exhibit translational motion coupled with frequent repositioning of particles within the group. The

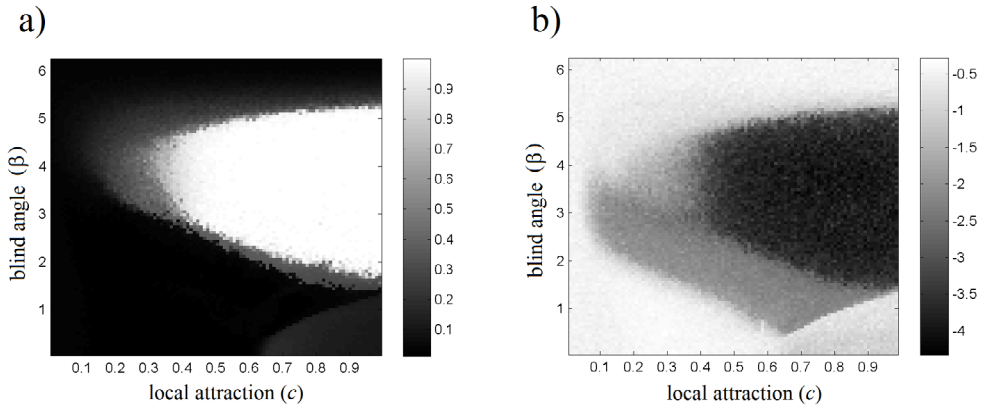

Fig. 3. Measuring the alignment and non-flatness in simulations of the 3D model. a) The result of measuring the alignment. We see several well defined regions in these plots and they cover the whole alignment spectrum. The white region in the middle has very high alignment, the black region for small c and β have almost no alignment and the rest of the regions have intermediate alignment values, ranging from low (dark gray) to fairly high (light gray). b) The result of measuring non-flatness. The general structure of this figure is similar to a) and many regions here have the same shape and location. We see that the dark gray region in the lower right corner of figure a) corresponds to a light gray region here, indicating that the structure is three dimensional, and that the white region in figure a) corresponds to a very dark gray region here, indicating that it is very flat. Similar to the alignment in figure a) we have several regions of intermediate non-flatness with dark to dark gray being moderately flat and light gray to white non-flat.

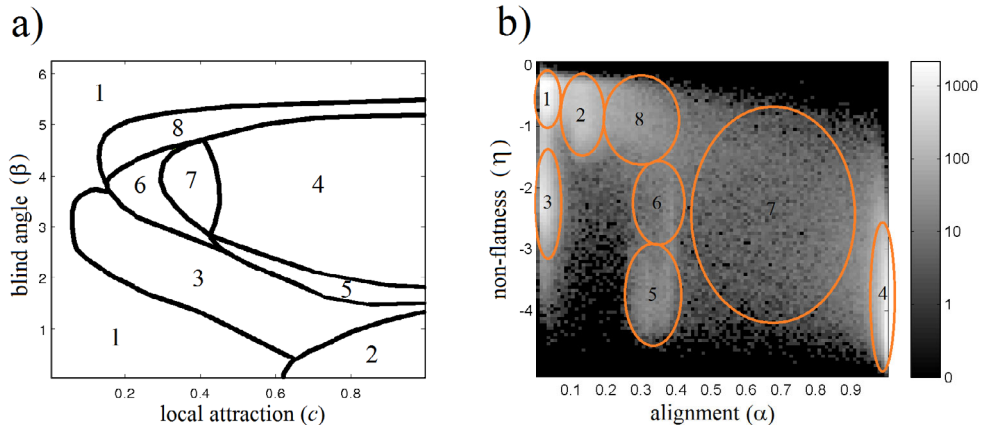

Fig. 4. Phase- and classification diagrams for the 3D system. a) Phase diagram with $c \in [0, 1]$ and $\beta \in [0, 2\pi]$ constructed by superimposing Figs. 3a and 3b. 1. No group, 2. Swarm (α low, η high), 3. Mill (α low, η low), 4. String (α high, η low), 5. Smaller figure of eight (α intermediate, η low), 6. Larger figure of eight (α intermediate-high, η low-intermediate) In the leftmost part of region 6 and further to the left of it we find rotating chains (α low, η intermediate-high), 7. Transition region between string and figure of eight, 8. Transition region between no group and unstable figure of eight. b) Classifying/pinpointing each structure and major transition region in Fig. 4a in the (α, η). We ran 10000 simulations with (c, β) uniformly distributed in the plane and measured the number of occurrences in each (α, η) point.

type of groups produced in the 2D and 3D case are directly analogous, and the same set of parameters tend to produce the same type of groups in both dimensions. The dynamics and shape of the groups obtained is no longer well described by a simple diagram such as Fig. 4a. In addition to c and β, the repulsion parameters R_r and r and their relation to speed δ and interaction radius R_a affect the shape and dynamics of the groups in a nontrivial way. Furthermore, the relationship between the number of particles N and the strength of global attraction g play a role in group formation since they regulate the density of the particle aggregate. If the global attraction is too strong we get a globally induced swarm. If the global attraction is too weak the particles do not aggregate enough for any group to form.

Given that there are too many parameters for a systematic treatment, we used Fig. 4a as a guide and manually investigated the parameter space. In this way we found five typical groups in the presence of repulsion: rigid translationally moving "flying-crystal" groups (Fig. 5a), translationally moving groups with frequent internal rearrangement of the particles (Fig. 5b), long strings/tubes (Fig. 5c), mills (Fig. 5d), and swarms (not shown here). Movie 2 shows the typical groups in the 2D model, and Movie 3 shows the groups in the 3D model.

We can make a number of observations about how the parameters determine shape and dynamics of the groups. For example, given a set of parameter values that produce a string/tube-like group, we can find some of the other typical shapes by adjusting c only. This is done for $\beta = 3.5$ in Figs. 5a–c. For $c >> d$ we get rigid round translationally moving groups (crystals) characterized by very high alignment, and for $c < d$ we get long twisting and turning strings/tubes. For c between these extremes groups of varying widths/lengths, and some with internal particle rearrangements occur ($c > d$). The length/width of a string/crystal can also be adjusted by varying the speed δ. Increasing δ typically gives longer thinner strings/crystals and decreasing δ gives shorter wider strings/crystals.

Formation of mills and tori typically occur when $c \approx d$, but also depend on the density induced by the choice of N and g. Milling tendency is also affected by β. If $c > d$ and $\beta << \pi$ swarms are observed, and for $\beta >> \pi$ often no group forms, but in between these extremes mills are observed and the width of the mill decreases with increasing β. These conditions are similar to those for mill formation in the absence of repulsion (Fig. 4a).

In order for the shapes in Fig. 5 to form, the repulsion parameters R_r and r are of key importance. Relatively large R_r ($\approx R_a$) and small r (< 0.5) produce smooth fluid-like internal particle movements that damps out perturbations, and relatively small R_r ($\approx R_a/2$) and large r (> 0.5) produce non-smooth internal rearrangements of particles, and perturbations propagate through the group. If these perturbation are too strong they may break the group apart.

In addition to the typical groups depicted in Fig. 5 we see hybrids of these. For many parameter values, we see groups switch between these different group types. For example, choosing parameters close to those in region 5 and 6 in Fig. 4a and using them in the attraction-repulsion model we often observe hybrids of mills and swarms that exhibit some degree of translational motion due to the presence of aligned subgroups within the larger group. We also observe groups switching between translational motion and stationary milling (Movie 4).

3 Discussion

In the absence of repulsion, increasing the dimension from 2D to 3D and replacing the periodic boundary conditions with a weak global attraction term does not significantly change the behavior of the model from that reported in [30]. The same

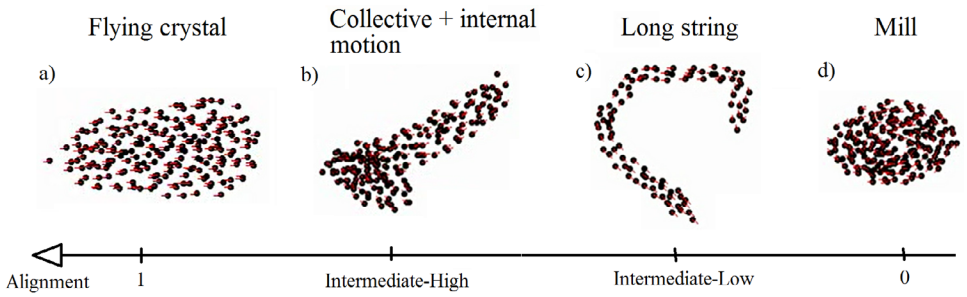

Fig. 5. The different typical groups seen in the 2D and 3D attraction-repulsion model. a) Rigid flying crystal. b) Crystal with collective and internal dynamics. c) Long string. d) Mill/torus. See Table 1 for the typical parameters used in the attraction-repulsion simulations, Movie 2 for 2D, and Movie 3 for 3D.

type of groups are seen in all cases: strings, mills, rotating chains, figure of eights and swarms. The diagram in Fig. 4a provides a description of group formation in the 3D case depending on c and β. However, stochasticity and initial conditions may affect the outcome and in practice several groups can be observed for the same parameter values [30]. This dependence on the initial conditions motivated using the median rather than the mean of the alignment and non-flatness measure in Fig. 3. The median better measures the shape of the most likely simulation outcome.

Self-propelled particle models based on attraction alone can produce a variety of group types even when repulsion is added. Stable figure of eights are no longer seen, however the groups depicted in Fig. 5 appear instead. The fact that this model produces the three standard groups, as well as translationally moving groups exhibiting frequent internal repositioning of particles, suggests that it may be used to model several natural flocks. In particular, some previously thought to require more elaborate models including an alignment term. For example, surf scoters [15,16] and fish [43–45]. In addition, the model produces groups that switch between translational motion and stationary milling (Movie 4). This is a key feature observed in experiments with golden shiners, and the attraction-repulsion-alignment model currently used to model these experiments does not produce such switching behavior in simulations [18]. Ongoing work include adapting the attraction-repulsion model presented here to model these golden shiner experiments.

To our knowledge no other attraction-repulsion model can produce groups posessing all the above mentioned properties. Two models [28,29] stand out as potentially capable of producing translationally moving groups with frequent internal repositioning of particles. These also share the feature of having a positional/heading update rule that is a linear combination of current heading and a social interaction term with the model presented here. However, the social interaction terms differ. In [28] it consists of one pursuit part (attraction) and one escape term (repulsion). In [29] it is "a sum of linear springlike forces", pushing particles apart if closer than a certain equilibrium distance, and pulling them together if further apart. Additional differences to our model include particles being polar ($\beta = \pi$) in [28], and in obtaining the results explicitly presented in [29] particles interact with a fixed set of other particles (producing regular structures). The model in [28] can generate the three standard groups, and seem able to generate repositioning of particles within translationally moving groups (See the e+p case in (Fig. 1, [28])). The model in [29] produces three very interesting active crystal type groups of various shapes (Hexagonal, rodlike, and square). Two of which reportedly exhibit translational motion coupled with internal motion (Fig. 1 AC, [29]). It is plausible that removing the fixed interaction topologies

in [29] may produce translationally moving groups exhibiting frequent internal repositioning of particles, but at present that has not been explicitly shown. Additionally, neither of these models have been shown to produce switching between group types.

While both alignment-based and attraction-based models can generate groups that look like natural flocks and schools, a comparison at the global level alone cannot distinguish which of these mechanisms plays the primary role in individual interactions [46,47]. Recent studies of individual interactions of mosquito fish [48] and golden shiners [49] suggest that an emphasis should be placed on attraction. These fish turn towards the position of their neighbors and decelerate to avoid collisions. Another species of fish, barred flagtails, do appear to exhibit alignment responses [50]. However, the method of data analysis differs between the former studies, which primarily rely on data-driven visualization of interactions, and the latter study, which explicitly fits a specific model to the data. This model fitting approach is also adopted in the above mentioned study of surf scoters [15]. If the model fitting is performed primarily when there is a high degree of alignment between individuals, it might lead to alignment being incorrectly inferred from the data. In general, investigating a near-equilibrium group structure is problematic for parameter inference because it provides an insufficiently wide range of configurations between individuals [51]. It would be interesting therefore to compare the fit of attraction-repulsion models with those alignment models already fit to the data in a rigorous manner, such as in [52]. In general, although we do not expect all animal interactions to be mediated by attraction-repulsion only, we do think that these types of interaction provide a parsimonious explanation for many aspects of collective motion.

In this study we have limited ourselves to small groups (≤ 100). We motivate this by the fact that many naturally occuring groups are small, and that many interesting data sets were collected with relatively few individuals [15,18,45,48–50,52]. In addition, we use metric, rather than topological, interactions here. In part because the original local attraction model [30] we extended here employed metric interactions, and also because several phenomena we plan to model using the framework presented here have been modeled by metric alignment-based models previously [15,16,18,50]. Future work also include comparing the three-dimensional version of our attraction-repulsion model with established models for the large starling flocks described by [8,53]. For example [32,41,42]. However, that will require us to use more particles (484-2630) and likely replace the metric interactions with topological interactions.

On a technical note, our study of the attraction-repulsion model together with recent work by [37] suggests that there is a direct correspondence between the relative strength of local attraction c and the blind angle β with respect to structure formation. More specifically, similar shapes can be obtained either by keeping β fixed and varying c or varying β and keeping c fixed. We found that by keeping β fixed we could systematically change the width/length/roundness by changing c alone and observed that the width (length) of the group decreases (increases) with increasing β. The latter agree with the corresponding findings in [37] where β is the primary parameter of interest rather than c as in this paper. Future work will include investigating this correspondence in detail, since it might allow us to simplify the attraction-repulsion model further.

4 Model and methods

4.1 Model description

We begin with a description of the model presented in [30]. N particles move with average speed δ on a torus (an $L \times L$ square with periodic boundary conditions).

The position of particle i at time t is denoted by $P_{i,t}$ and the unit vector indicating direction is denoted $\hat{D}_{i,t}$. Initially each particle is assigned a random direction and a random position. On each time step each particle interacts with neighboring particles located within a distance of R_a except those positioned in the "blind zone" behind it specified by the angle β and defined as follows. Particle i at position P_i with normalized heading $\hat{D}_i$ will not be influenced by particle j at position P_j if

$$\arccos\left(\frac{P_iP_j \cdot \hat{D}_i}{|P_iP_j|}\right) < \frac{\beta}{2}, \tag{1}$$

where P_iP_j is the vector from particle j to particle i. The only social interaction in the model is an attraction to the center of mass of the neighboring particles outside this blind zone, and $\hat{C}_{i,t}$ is used to denote the normalized direction toward this center of mass. Particle i's heading in the next time step $D_{i,t+1}$ is a linear combination of its direction in the current time step $\hat{D}_{i,t}$, the center of mass of its current neighbors $\hat{C}_{i,t}$ and an error term $\hat{\epsilon}_{i,t}$. The model parameters d, c and e determine the relative strength of each component and the new heading of particle i is

$$D_{i,t+1} = d\hat{D}_{i,t} + c\hat{C}_{i,t} + e\hat{\epsilon}_{i,t}. \tag{2}$$

A uniformly distributed random variable $\zeta \in [-\kappa/2, \kappa/2]$ is introduced to allow for variation in speed and the new position of particle i is given by

$$P_{i,t+1} = P_{i,t} + \delta(1 + \zeta_{i,t})\hat{D}_{i,t+1}. \tag{3}$$

Here we modified the above model to increase its biological plausibility and to make sure that the periodic boundary conditions used in [30] did not play a significant role in group formation. The periodic boundary conditions were replaced by a weak linear global attraction term G. Denoting the center of mass of all the particles GCM_t the global attraction term for particle i is given by

$$G_{i,t} = GCM_t - P_{i,t}.$$

Including this new term particle i's heading at time $t + 1$, given the state at time t, is given by

$$D_{i,t+1} = d\hat{D}_{i,t} + c\hat{C}_{i,t} + gG_{i,t} + e\hat{\epsilon}_{i,t}, \tag{4}$$

and the position is updated according to equation 3. Note that, unlike $\hat{C}_{i,t}$, $G_{i,t}$ is not normalized, so attraction to the global centre of mass increases with distance.

To include repulsion we used a distance dependent version of the standard function found in [24,27]. In contrast to these hierarchical zone models we aim to have overlapping repulsion and attraction zones, so that repulsion and attraction compete at intermediate distances. This assumption reflects the fact that some flocking animals adjust their headings well in advance to avoid collisions and find their position in the flock [48]. We want the repulsive effect on a particle from a distant neighbor to be small (planning ahead) and a nearby neighbor to be large (when planning ahead fails), inspired by the continuous models reviewed in [54]. The repulsion term is defined as follows. If particle i has n neighbors within a distance of R_r at positions $P_{1,t}, .., P_{n,t}$ the repulsive force on i is given by

$$F_{i,t} = \sum_{j=1}^{n} \frac{P_{i,t} - P_{j,t}}{|P_{i,t} - P_{j,t}|^3}. \tag{5}$$

The repulsive force is then added with weight r to the linear combination giving the new heading

$$D_{i,t+1} = d\hat{D}_{i,t} + c\hat{C}_{i,t} + gG_{i,t} + rF_{i,t} + e\hat{\epsilon}_{i,t}. \tag{6}$$

Extending the model from two to three dimensions model does not change its mathematical expression. All the equations in 3D are the same but with 3-vectors instead of 2-vectors and the blind sector is replaced by a blind cone. The model interactions are summarized in Fig. 1. See Table 1 for a brief description and typical values of the parameters.

4.2 Attraction only

Initially we explored the model without repulsion using Fig. 6 in [30] as a guide. This allowed us to locate the typical structures arising in the 2D and 3D models. Once found we verified the stability of each structure using simulations of 10000 timesteps. To quantify our model results we use two measures of flock structure and dynamics. The first is the well known alignment (or polarization) measure [21] defined by

$$\alpha = \frac{1}{N}\left|\sum_{i=1}^{N} \hat{D}_i\right| \tag{7}$$

where $\hat{D}_i$ is the normalized heading of particle i. It measures the extent to which the particles are moving in the same direction. It is 1 when all particles are moving in exactly the same direction, and it is small (≈ 0) when the particles are moving in very different directions (for example when moving on a mill).

In 2D the alignment and group size was enough to classify groups [30], but in 3D we require another measure to be able to distinguish swarms from mills and show that there are different types of figure of eight. This measure relates to the flatness of the structure. To calculate it we first fit a two-dimensional second order polynomial surface to the positions of all the particles using the *fit* command *poly22* from the Matlab Curve Fitting Toolbox [55].

The non-flatness η is then defined by

$$\eta = \log \frac{\sqrt{\sum_{i=1}^{N} \delta_i^2}}{\sqrt{\sum_{i=1}^{N} \rho_i^2}}, \tag{8}$$

where δ_i is the distance from particle i to the nearest point on the fitted surface and ρ_i is the distance from particle i to the group's center of mass. The reason for scaling with the sum of the ρ_i's is to make the measure independent of the size of the group. A flat structure (e.g. a mill) will have η relatively low and a non-flat structure (e.g. a swarm) will have η relatively large.

In generating the diagrams in Fig. 3 we used 50 particles and ran 30 simulations for each (c, β)-pair, with a resolution of 100×100 pairs of parameter values. Each simulation was 300 time steps long and during the last 50 time steps we measured alignment and non-flatness on every other time step. The median of these 25 measurements was output as the result of a single simulation and then the reported alignment and non-flatness were given by the median of these 30 simulation outputs. To get feasible structure formation within 300 time steps we start the simulations with compact swarms of particles. Specifically, initially the particles were distributed randomly in a $30 \times 30 \times 30$-cube with random headings. To be sure that we were measuring the main structure created by the particles, and not any extra structure

created by particles which had escaped the main group, we calculated the position of the global center of mass using only half of the particles, excluding the quarter with the largest and smallest coordinate values respectively. The other parameters were set to $R_a = 10, \delta = 1, d = 1 - c, e = 1/60$, $\kappa = 1/5$ and $g = 1/20$. Once we had created the diagram on the basis of these relatively short simulations, we verified its accuracy by probing each region of parameter space manually using simulations of 10000 timesteps. This allowed us to check that the correct structures formed and to analyze their stability properties.

4.3 Attraction and repulsion

To investigate the attraction-repulsion model we ran simulations of 10000 timesteps to probe the parameter space, but did not systematically run through all parameter values. Due to strong dependence on several parameters in addition to c and β we were not able to construct a diagram similar to Fig. 4a for this version of the model. Instead, using the attraction only case (Fig. 4a) as a guide, we manually investigated the parameter space in order to make an inventory of the groups present.

This work was in part funded by an ERC starting grant to David Sumpter (ref: IDCAB).

References

1. E. Shaw, American Scientist **66**, 166 (1978)
2. N. Newlands, Shoaling dynamics and abundance estimation: Atlantic bluefin tuna (thunnus thynnus), Ph.D. thesis, University of British Columbia, 2002
3. F. Heppner, Bird-Banding **45**, 160 (1974)
4. A. Procaccini, A. Orlandi, A. Cavagna, I. Giardina, F. Zoratto, D. Santucci, F. Chiarotti, C. Hemelrijk, E. Alleva, G. Parisi, C. Carere, Animal Behaviour **82** (2011)
5. J. Parrish, W. Hamner (eds.), Animal Groups in Three Dimensions (Cambridge University Press, 1997)
6. T. Pitcher, Behaviour of Teleost Fishes, 2nd Edition (Chapman and Hall, 1993)
7. B. Partridge, J. Comp. Physiol. **144**, 313 (1981)
8. M. Ballerini, N. Cabibbo, R. Candelier, A. Cavagna, E. Cisbani, I. Giardina, A. Orlandi, G. Parisi, A. Procaccini, M. Viale, V. Zdravkovic, Animal Behaviour **76**, 201 (2008)
9. P. Friedl, D. Gilmour, Nature **10**, 445 (2009)
10. L. Cisneros, R. Cortez, C. Dombrowski, R. Goldstein, J. Kessler, D. Gilmour, Exper. Fluids **43**, 737 (2007)
11. C. Breder, Ecology **35**, 361 (1954)
12. P. Conder, Ibis **91**, 649 (1949)
13. J. Emlen, The Auk **69**, 160 (1952)
14. R. Miller, W. Stephen, Ecology **47**, 323 (1966)
15. R. Lukeman, X. Li, L. Edelstein-Keshet, PNAS **107**, 12576 (2010)
16. R. Lukeman, Modeling collective motion in animal groups: from mathematical analysis to field data, Ph.D. thesis, 2009
17. A. Cavagna, A. Cimarelli, I. Giardina, G. Parisi, R. Santagati, F. Stefanini, M. Viale, PNAS **107** (2010)
18. K. Tunstrøm, Y. Katz, C.C. Ioannou, C. Huepe, M.J. Lutz, I.D. Couzin, PLoS. Comput. Biol. **9** (2013)
19. I. Aoki, Bull. Jpn. Soc. Fish. **48** (1982)
20. A. Huth, C. Wissel, J. theor. biol. **156**, 365 (1991)
21. T. Vicsek, A. Czirók, E. Ben-Jacob, I. Cohen, O. Shochet, Phys. Rev. Lett. **75**, 1226 (1995)

22. G. Grégorie, H. Chaté, Y. Tu, Physica D **181** (2003)
23. A. Czirók, H. Stanley, T. Vicsek, J. Phys. A. **30**, 1375 (1997)
24. I. Couzin, J. Krause, R. James, G. Ruxton, N. Franks, J. Theor. Biol. **218**, 1 (2002)
25. A. Czirók, M. Vicsek, T. Vicsek, Physica A **264**, 299 (1999)
26. M. D'Orsogna, Y. Chuang, A. Bertozzi, L. Chayes, Phys. Rev. Lett. **96** (2006)
27. A. Wood, G. Ackland, Proc. R. Soc. B **274**, 1637 (2007)
28. P. Romanczuk, I. Couzin, L. Schimansky-Geier, Phys. Rev. Lett. **102** (2009)
29. E. Ferrante, A.E. Turgut, M. Dorigo, C. Huepe, Phys. Rev. Lett. **111** (2013)
30. D. Strömbom, J. Theor. Biol. **283**, 145 (2011)
31. D. Strömbom, R. Mann, A. Wilson, S. Hailes, A. Morton, D. Sumpter, A. King, J.R. Soc. Interface **11** (2014)
32. M. Camperi, A. Cavagna, I. Giardina, G. Parisi, E. Silvestri, Interface Focus **2**, 715 (2012)
33. T. Vicsek, A. Zaferidis, Phys. Reports **517**, 71 (2012)
34. W.L. Romey, Ecological Modelling **92**, 6577 (1996)
35. P. Romanczuk, L. Shimansky-Geier, Interface Focus **2**, 746 (2012)
36. Y. Sugiyama, Group formation of self-driven system. application of 2-dimensional optimal velocity model (2008), presentation
37. W.L. Romey, J.M. Vidal, Ecological Modelling **258**, 9 (2013)
38. H. Levine, W.J. Rappel, Phys. Rev. E (2000)
39. W. Ebeling, L. Schimansky-Geier, Eur. Phys. J. Special Topics **157**, 17 (2008)
40. J. Park, Collective motion in 3d and hysteresis, Master's thesis, Uppsala University (2011)
41. H. Hildenbrandt, C. Carere, C. Hemelrijk, Behavioral Ecology **21**, 1349 (2010)
42. N. Bode, D. Franks, A. Wood, J.R. Soc. Interface **8**, 301 (2011)
43. C. Hemelrijk, H. Kunz, Behavioral Ecology **16**, 178 (2005)
44. C. Hemelrijk, H. Hildenbrandt, Ethology **114**, 245 (2008)
45. C. Hemelrijk, H. Hildenbrandt, J. Reinders, E. Stamhuis, Ethology **116**, 1099 (2010)
46. D. Sumpter, R. Mann, A. Perna, Interface Focus **2**, 764 (2012)
47. U. Lopez, J. Gautrais, I. Couzin, G. Theraulaz, Interface Focus **2**, 693 (2012)
48. J. Herbert-Read, A. Perna, R. Mann, T. Schaerf, D. Sumpter, A. Ward, PNAS **108**, 18726 (2011)
49. Y. Katz, K. Tunstrøm, C. Ioannou, C. Huepe, I. Couzin, PNAS **108**, 18720 (2011)
50. J. Gautrais, F. Ginelli, R. Fournier, S. Blanco, M. Soria, H. Chaté, PLoS Comput. Biol. **8** (2012)
51. R. Mann, PLoS ONE **6** (2011)
52. R. Mann, A. Perna, D. Strömbom, R. Garnett, J. Herbert-Read, D. Sumpter, A. Ward, PLoS Comput. Biol. **9** (2013)
53. M. Ballerini, N. Cabibbo, R. Candelier, A. Cavagna, E. Cisbani, I. Giardina, V. Lecomte, A. Orlandi, G. Parisi, A. Procaccini, M. Viale, V. Zdravkovic, PNAS **105** (2008)
54. A. Mogilner, L. Edelstein-Keshet, L. Bent, A. Spiros, J. Math. Biol. **47**, 353 (2003)
55. Matlab, Matlab Curve Fitting Toolbox™ User's Guide (2012)